phys. stat. sol. (a) **197**, No. 3, 648–661 (2003) / **DOI** 10.1002/pssa.200303115

An experimental study of strongly modified emission in inverse opal photonic crystals

A. Femius Koenderink[*], **Lydia Bechger, Ad Lagendijk,** and **Willem L. Vos**

Complex Photonic Systems, Department of Applied Physics and MESA$^+$ Research Institute, University of Twente, P.O. Box 217, 7500 AE Enschede, The Netherlands[**]

Received 15 October 2002, revised 21 March 2003, accepted 28 March 2003
Published online 20 June 2003

PACS 42.25.Fx, 42.50.Ct, 42.70.Qs, 81.05.Zx

We present the first experiments that demonstrate strong angle-independent modification of spontaneous emission spectra from laser dyes in photonic crystals, made of inverse opals in titania. We show that both the fluorescence quantum efficiency and weak disorder play a key role in interpreting the experimental data. We compare the angle-independent emission spectra of dye in photonic crystals with spectra from such crystals with much smaller lattice spacings, for which emission is in the long wavelength limit. The ratio of emission power spectra shows inhibition of emission up to a factor ~ 5 over a large bandwidth of 13% of the first order Bragg resonance frequency. The inhibition shifts to increasing wavelength with the lattice parameter, confirming the photonic nature of the phenomenon. The center frequency and bandwidth of the inhibition agree with the calculated total density of states, but the measured inhibition of the vacuum fluctuations is much larger. This result is confirmed by experiments using different dyes. We likely probe the strongly modulated local photonic density of states, due to the spatially nonuniform distribution of dye molecules over the unit cell.

1 Introduction

Since the development of cavity quantum electrodynamics (QED) over the last decades, it has been recognized that fundamental atom-radiation interactions may be controlled by tailoring the electromagnetic mode density [1]. Numerous cavity QED experiments have demonstrated the effects of manipulating vacuum fluctuations. Prime examples are reductions and enhancements of spontaneous emission rates and energy transfer processes, cavity induced energy level shifts, and Van der Waals and Casimir forces [1–5]. Cavity QED experiments are generally limited to narrow spectral bandwidths, and small spatial volumes, i.e., near the center of the cavity. It is highly desirable to manipulate vacuum fluctuations over large bandwidths and extended spatial volumes in solid state systems, as proposed for photonic band gap materials [6–8].

Complete suppression of vacuum fluctuations is expected in the case of a photonic band gap, a frequency range for which no electromagnetic modes exist. A photonic band gap arises from strongly coupled Bragg diffractions in periodic dielectric structures with periodicity comparable to the wavelength of interest. The fabrication and optical properties of such photonic crystals currently receive much interest [7, 8]. A photonic band gap, and the associated complete suppression of the electromag-

[*] Corresponding author: e-mail: a.f.koenderink@utwente.nl, Phone: +31 53 489 5390, Fax: +31 53 489 5394
[**] Web address: www.photonicbandgaps.com

 0031-8965/03/19706-0648 $ 17.50+.50/0

netic mode density is hard to realize. In pioneering experiments on 3D photonic crystals, the inhibition was limited to a few percent by the small dielectric contrast [9–12]. Significant inhibition of spontaneous emission by strongly photonic crystals has not yet been reported, although several authors have unfortunately (mis)interpreted stop gaps in emission as such [13–16]. A change of the spontaneous emission rate of a dipole is clearly an angle-integrated property, that can not be addressed by measuring the emission spectrum in one particular direction without further justification. Furthermore, a main complication is to find a proper reference system to which emission properties inside a photonic crystal can be compared, and to properly account for the role of luminescence quantum efficiency in the experiment. We have recently reported the first broadband inhibition of spontaneous emission, realized in strongly photonic titania air sphere crystals [17]. In this paper, we discuss the angle-independent spontaneous emission power from dyes in photonic crystals, paying particular attention to our choice of reference system, the impact of luminescence quantum efficiency, and the role of disorder in the interpretation of our data. This work opens up new research opportunities for studies of quantum optical phenomena in condensed matter environments.

2 Fermi's Golden Rule and quantum efficiency

The aim of the experiment presented in this paper, is to verify the degree to which spontaneous emission is influenced by the total or local photonic density of states (DOS, resp. LDOS) for frequencies in the pseudo gap of titania inverse opals [18, 19]. The pseudo gap is the range of frequencies starting at and just above the L-gap, the stop gap associated with the lowest order Bragg diffraction (see Fig. 1). The local density of states $N_{\mathrm{rad}}(\boldsymbol{r}, \boldsymbol{d}, \omega)$ affects the radiative decay rate $\Gamma_{\mathrm{rad}}(\boldsymbol{r})$ of a dipole transition with transition frequency ω at dipole position $\boldsymbol{r}$ through Fermi's Golden Rule according to

$$\Gamma_{\mathrm{rad}}(\boldsymbol{r}) = \frac{\pi\omega\mu^2}{3\hbar\epsilon_0} N_{\mathrm{rad}}(\boldsymbol{r}, \boldsymbol{d}, \omega)\,,$$

where $\boldsymbol{d}$ is the transition dipole orientation, and μ the transition dipole moment [20]. The relevance of the local radiative density of states (LDOS) N_{rad} for spontaneous emission in photonic systems, was first pointed out by Sprik, van Tiggelen and Lagendijk [18]. The local radiative density of states

$$N_{\mathrm{rad}}(\boldsymbol{r}, \boldsymbol{d}, \omega) = \frac{1}{\epsilon(\boldsymbol{r})} \sum_{n,\boldsymbol{k}} 2\omega\delta(\omega^2 - \omega_{n,\boldsymbol{k}}^2)\, |\boldsymbol{d} \cdot \boldsymbol{\Lambda}_{n,\boldsymbol{k}}(\boldsymbol{r})|^2 \tag{1}$$

not only entails counting the eigenfrequencies $\omega_{n,\boldsymbol{k}}$ of the photonic Bloch modes (summed over bands n and wave vector $\boldsymbol{k}$ in the first Brillouin zone), but also involves the complete set of electromagnetic mode functions $\boldsymbol{\Lambda}_{n,\boldsymbol{k}}(\boldsymbol{r})$. These are the orthonormal eigenfunctions of the symmetrized Maxwell wave equation ($\epsilon^{-1/2}\nabla \times \nabla \times \epsilon^{-1/2}\boldsymbol{\Lambda} = \omega^2/c^2\boldsymbol{\Lambda}$), and can be determined easily from the E- or H-field Bloch modes. Given the spatially periodic dielectric constant $\epsilon(\boldsymbol{r})$, these Bloch modes can be calculated by plane wave methods [21, 22]. In terms of the H-field eigenmodes $\boldsymbol{H}_{n,\boldsymbol{k}}(\boldsymbol{r})$ for instance, one finds $\boldsymbol{\Lambda}_{n,\boldsymbol{k}}(\boldsymbol{r}) = (\nabla \times \boldsymbol{H}_{n,\boldsymbol{k}}(\boldsymbol{r}))/(\sqrt{\epsilon(\boldsymbol{r})}\, i\omega_{n,\boldsymbol{k}})$. Intricacies of the local density of states have been dealt with elsewhere [23]; here we only summarize some important points concerning spontaneous emission. It is important to realize that the total density of states

$$N(\omega) = 2\omega \sum_{n,\boldsymbol{k}} \delta(\omega^2 - \omega_{n,\boldsymbol{k}}^2) \tag{2}$$

is *the unit cell average* of the local density of states $\epsilon(\boldsymbol{r})\, N_{\mathrm{rad}}(\boldsymbol{r}, \boldsymbol{d}, \omega)$, (averaged over dipole orientation). Hence (1) a gap in the total DOS implies a gap in the LDOS, independent of the position of the emitter in the unit cell. Furthermore (2) the emission rate of an emitter in a photonic crystal may depend strongly on the position of the emitter in the unit cell. Also (3) in the absence of a gap in the total DOS, there may still exist positions in the unit cell for which the local density of states has a gap, indicating that spontaneous emission can be completely inhibited for carefully placed emitters.

The most obvious experiment to probe the DOS or LDOS consists of taking a two level system, keeping the 'atom' part (ω and μ) fixed, and comparing the decay rate Γ of this source at a well defined position in the crystal with the decay rate of the source in a reference system with a known local density of states. For total DOS characterization, one would need to average the result over all source sites and orientations in the crystal unit cell. Such a measurement is based on having (1) a source with quantum efficiency near unity, (2) a chemically identical reference system with controlled LDOS, and (3) knowledge of or control over the location of the luminescent sources. In Sections 2 and 3, we will explain the intricacies associated with the source quantum efficiency and discuss the optimal choice of reference satisfying these criteria.

In a time-resolved fluorescence measurement one records the excited state population at time t, which decays with a decay rate Γ_{tot}. This total decay rate is determined by the sum of both the radiative and all nonradiative decay channels, and reads $\Gamma_{\mathrm{tot}} = \Gamma_{\mathrm{rad}} + \Gamma_{\mathrm{NR}}$. Here the nonradiative decay rate Γ_{NR} results from all competing nonradiative decay channels. Evidently, changes in Γ_{rad} can only be determined from a dynamic measurement if the quantum efficiency $\eta = \Gamma_{\mathrm{rad}}/\Gamma_{\mathrm{tot}}$ is of order unity. At the risk of obscuring the discussion, we note that the quantum efficiency *depends on the source position* in the case of a spatially inhomogeneous local DOS, unless nonradiative decay can be ruled out completely.

Naively, one might expect that the total emission power in a cw experiment may also reflect the local density of states, since a gap in the LDOS would obviously result in a total absence of emitted photons. However, closer examination shows that the total emission power is not indicative of the LDOS for sources with near unit quantum efficiency. We consider an effective two-level system that is pumped at a constant rate P. The excited state population is governed by

$$\frac{\mathrm{d}N_2}{\mathrm{d}t} = P - \Gamma_{\mathrm{tot}} N_2$$

and amounts to $N_2 = P/\Gamma_{\mathrm{tot}}$ in the stationary case. The number of photons I emitted per unit time is simply the fraction η of decay instances $\Gamma_{\mathrm{tot}} N_2$ in which a photon is actually emitted, i.e., $I = \eta \Gamma_{\mathrm{tot}} N_2 = \eta P = P\Gamma_{\mathrm{rad}}/\Gamma_{\mathrm{tot}}$. For unit quantum efficiency this relation simply states that every incident pump photon is converted into an emitted photon and implies that the emitted power at fixed pump rate is not related to the DOS. Still, this result apparently conflicts with the notion that the emitted power vanishes if the source frequency matches a gap in the DOS. This controversy is easily resolved by noting that a constant nonzero pump rate can not be achieved for identically zero decay rate, i.e., in the case of a transition in the photonic band gap and unit quantum efficiency. Then, the pump rate drops to zero as soon as all light sources are excited. Generally, this saturation argument comes into play for pump energy densities W_D such that the absorption rate per emitter $(W_D c/\hbar\omega)\,\sigma_a$ (where σ_a is the absorption cross section) is comparable to or larger than the decay rate Γ_{tot}. This regime is not met in the experiments reported in this paper, but is automatically met if $\Gamma_{\mathrm{tot}} = 0$. An alternative perspective orginates from classical electromagnetic theory for a radiating dipole antenna [24]. One may interpret a constant pump rate as taking a dipole antenna into which a constant power is fed and which therefore radiates at a constant output power. As the local density of states decreases, a larger dipole current is needed to input the same power. For a frequency in the gap an infinite current would be needed to drive the dipole at the specified power. The converse notion is at the heart of finite difference time domain calculations [25], where the emitted power at given dipole current is used to determine the LDOS.

A most surprising result is obtained if one considers a system of low quantum efficiency ($\eta \ll 1$). Then, the total decay rate $\Gamma_{\mathrm{tot}} = \Gamma_{\mathrm{NR}}(1 + \eta + \mathcal{O}(\eta^2))$ is completely determined by the nonradiative decay channels. The emitted power $I = P\Gamma_{\mathrm{rad}}/\Gamma_{\mathrm{tot}} \cong P\Gamma_{\mathrm{rad}}/\Gamma_{\mathrm{NR}}$ is therefore an excellent signature of the radiative decay rate if it is referenced to a system with the same nonradiative decay channels. In conclusion, cw and time-resolved measurements can be used in complementary cases to probe the photonic density of states. For efficient sources the emission power only reflects the pump rate and the decay time reveals the LDOS. For inefficient sources on the other hand, the emission power reflects the LDOS, but the total decay time is not affected by the photonic environment.

3 Nonphotonic reference

The choice of reference host in which to embed the chosen luminescent species is of prime importance for a comparison with the photonic system. It is essential that the reference system provides the same chemical environment as the photonic system to ensure an unchanged transition dipole moment, the same nonradiative decay rate and the same inhomogeneous broadening. Lifetime changes observed in several time-resolved experiments in which the refractive index mismatch in a photonic system was tuned by infilling with different solvents were rather due to changes in the transition dipole moment or chemical interactions [26], than to photonic effects [9, 10]. Indeed it is well known that, e.g., the polarity of a solvent influences the emission properties of organic dyes. Furthermore it is clear from the discussion above, that especially in the case of a cw measurement, the reference material should provide the same nonradiative decay rate Γ_{NR} in order to make a comparison of emitted powers possible.

It is especially beneficial to choose a luminescence species with a large inhomogeneous linewidth if the emission power of inefficient sources is to be probed. Sources with a narrow *homogeneous* linewidth should be chosen to ensure that each emitter probes the local DOS in a frequency window narrow compared to the spectral features of the LDOS. If an ensemble of sources is chosen with a large inhomogeneous linewidth, many frequencies can be probed independently but simultaneously. In addition, a large inhomogeneous linewidth facilitates comparison of the emitted power from photonic and reference systems, independent from differences in pump efficiency. The emitted power for the photonic and reference system can only be compared to obtain the variation due to the LDOS if differences in the pump rate are accounted for. A priori, this necessitates quantifying the detection- and pump efficiency for both the photonic and reference experiment. For an inhomogoneously broadened lineshape, the ratio of the photonic to the reference spectrum of inefficient sources

$$\frac{I_{\mathrm{photonic}}}{I_{\mathrm{reference}}} = \frac{P_{\mathrm{photonic}}}{P_{\mathrm{reference}}} \frac{\Gamma_{\mathrm{rad,\,photonic}}}{\Gamma_{\mathrm{rad,\,reference}}} = A \frac{\langle N_{\mathrm{rad,\,photonic}} \rangle\,(\omega)}{\langle N_{\mathrm{rad,\,reference}} \rangle\,(\omega)}$$

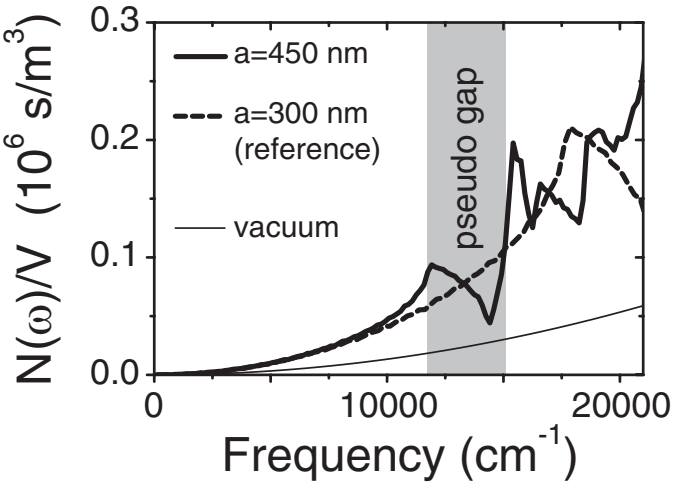

Fig. 1 Density of states $N(\omega)$ per volume V versus optical frequency calculated for titania inverse opals (26% material with $\epsilon = 6.5$) with two different lattice parameters. The DOS of the sample with the small lattice parameter $a = 300$ nm (dashed) is approximately quadratic in the frequency range of the pseudogap of the inverse opal with $a = 400$ nm (solid line). In this frequency range (shaded area), the crystal with small lattice parameter is an excellent reference. The DOS of vacuum (thin line) is also indicated. In the low frequency limit, the DOS of the titania samples differ from the vacuum DOS by a scaling factor n_{eff}^3. Here n_{eff} is the average refractive index of the crystals.

reveals the frequency dependence of the *ratio* of the photonic and reference local DOS (averaged over source positions and orientations, as indicated by $\langle . \rangle$) over a large frequency range. The constant of proportionality A contains the differences in pump- and detection efficiency, and can be eliminated if the ratio $\langle N_{\mathrm{rad,\,photonic}} \rangle (\omega) / \langle N_{\mathrm{rad,\,reference}} \rangle (\omega)$ is explicitly known at some specific frequency, particularly if the inhomogeneous spectrum of the photonic sample extends to frequencies below the window of photonic behavior.

Within the constraint of identical chemical composition, one may consider, e.g., disordered titania composites, such as powders or pulverized samples as suitable references for experiments on titania inverse opals. However, such a material would be highly multiply scattering [27], possibly giving rise to a strongly modulated and position dependent local DOS [28]. As Fig. 1 demonstrates, a titania inverse opal with a very small lattice constant on the other hand, is optimally suited as a reference environment. The band structure depends only on the normalized frequency $\omega a / 2\pi c$. A crystal with small lattice parameter a will therefore only be photonic for large frequencies. For sufficiently small lattice constant, the spectrum of the emitter will probe the long wavelength limit of such chemically identical crystals. In this limit the crystals behave as weakly scattering effectively homogeneous media, and provide a DOS with a quadratic frequency dependence typical for a medium with the effective refractive index of the titania inverse opals.

4 Experiment

We studied titania inverse opals with cubic lattice parameters $a = 430$ and 480 nm doped with the organic laser dye Rhodamine 6G (R6G), and with lattice parameter $a = 510$ nm doped with the organic laser dye Nile Blue [29]. The preparation and structural characterization of these fcc crystals of close packed air spheres in a titania matrix has been reported in Ref. [19, 30]. The strongly opalescent samples have overall dimensions of the order of millimeters and thicknesses of $\sim 200\,\mu$m, and are composed of high-quality crystal domains with diameters of $\sim 50\,\mu$m, as confirmed by small angle X-ray scattering [30]. Defects, displacements and polydispersity of the air spheres are inherited from the opal template. Wide angle X-ray diffraction has revealed the solid material to be polycrystalline anatase titania, with an average grain size of 20 nm, consistent with the $\lesssim$10 nm roughness observed for a wide range of lattice parameters a in small angle X-ray scattering [30]. The solid material is deposited in spherical shells surrounding close-packed air spheres [19]. Air spheres are connected by cylindrical windows at the contact points. The volume fraction of solid material contained in the shells is between 6 and 12%, leaving interstitial voids in between air spheres. The observed high dielectric constant of the anatase-titania backbone ($\epsilon = 6.25$ to 6.5 [30, 31]) makes these 'inverse opals' or 'air-sphere crystals' into some of the most strongly-photonic 3D crystals available for optical wavelengths. Recent experiments have shown single domain reflectivities up to 95% [32], exclusion of modes over up to 55% of all directions [33] and flattening of dispersion bands characteristic of strong photonic interaction [34].

The organic dyes R6G and Nile Blue feature emission spectra with a large inhomogeneous width of order 5000 cm^{-1}. The homogeneous linewidth is of order $\lesssim$170 cm^{-1}, as borne out by photon echo experiments [35], and cavity enhanced emission of dye in microspheres [4, 36]. In addition to the aforementioned 'photonic' samples, titania inverse opals with lattice spacing $a = 350$ nm were prepared as reference hosts. The reference crystals, manufactured along the same preparation route as the 'photonic' samples but starting from smaller template spheres, were doped with dye according to the same procedure used for the photonic samples. Explicitly, the R6G-doped samples were prepared by 30 min. immersion in a dilute $\sim 1\,\mu$mol solution of R6G in ethanol, followed by rinsing and drying. Nile Blue samples were similarly immersed for 24 h, rinsed and dried, using a 70 μmol solution of Nile Blue in ethanol. To select emission from the bulk of the photonic crystals, the dye adsorbed near the external sample surface was bleached by illuminating the crystals with an intense laser beam at the Bragg angle [37]. The exponential attenuation with depth into the sample of the pump beam due to Bragg diffraction, limits the bleaching to the first few crystal layers. Spectra were found to be

independent of observation angle prior to bleaching. Bleaching caused angle-dependent modifications of the spectral lineshapes to occur. The angle-dependence is due to stop bands that attenuate the spectra due to internal Bragg diffraction for frequencies and directions coincident with stop gaps in the dispersion relation [38]. Bleaching was monitored by the saturation of the stop gap depth in the $\alpha = 0^\circ$ emission spectrum, where α is the emission angle relative to the surface normal, which coincides with the 111 reciprocal lattice vector. Further bleaching only resulted in a decrease of the emission intensity. For the reference samples, surface bleaching was attempted using the 457 nm line of an Argon laser at normal incidence. Though the overall emission intensity at constant pump power decreased, spectra from the reference samples did not show drastic changes and did not develop an angular dependence due to the photobleaching, until the point where bleaching reduced the signal to nearly dark count rate. As the dye molecules are adsorbed onto the titania, our probe of the DOS is limited by the volume fraction of solid material to be less than 12% of the unit cell volume.

The dye in the crystals was excited with a *p*-polarized laser beam emitted by a cw Argon ion laser tuned to a wavelength of $\lambda = 488$ nm in the case of R6G-doped samples. For spectral measurements of emission from Nile-Blue doped samples, as well as for time-resolved fluorescence decay measurements *p*-polarized emission from a mode-locked frequency-doubled Nd^{3+} : YAG laser was employed. Figure 2 shows a schematic overview of the experimental setup. The actively mode-locked Nd^{3+} : YAG laser (Spectra Physics 3800) generated 12 W average output power in TEM_{00} mode in 100–150 ps pulses (full width at half maximum) at a 80MHz repetition rate. These pulses were shortened to 5–10 ps in a Spectra Physics 3595 fiber/grating pulse compressor to achieve a high power for second harmonic generation. The system was actively stabilized at a constant average power of $\sim$400 mW at 532 nm. In all experiments, the cw excitation power at the sample was below 10 μW focused to a spot of 30 μm in diameter. Samples were mounted on a goniometer allowing to vary the detection angle α relative to the surface normal. Stop gaps in the emission spectra were used as a quality check of the crystals. The position of the pump spot on the sample, and the alignment of the sample and beam relative to the goniometer axis were monitored and controlled to within 20 μm using a small long working-distance microscope. Fluorescence was imaged onto the entrance slit of a Carl

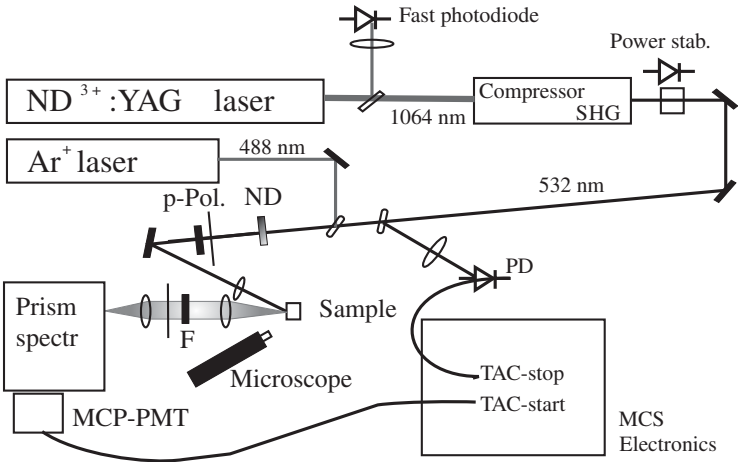

Fig. 2 Set up for time resolved and cw fluorescence experiments. Pulses from a mode-locked Nd^{3+} : YAG laser are pulse-compressed and frequency doubled. Mode locking is monitored by a fast photodiode, and the cw frequency-doubled power is actively stabilized. Part of the beam is split off onto a trigger diode (PD), while the remaining part is attenuated (ND filter), p-polarized, and focused onto the sample. Alignment of the sample is monitored using a long working distance microscope. Emission is focused onto the prims spectrometer entrance slit, filtered (F), detected by a microchannel plate photomultiplier tube (MCP-PMT), and recorded with a multichannel scaler (MCS). For cw measurements on R6G, the 488 nm line of an Argon laser was used.

Leiss monochromator equipped with a flint prism. The slit width was set to accommodate the low count rates due to the limited dye concentrations, providing a resolution of $\sim 100\,\mathrm{cm}^{-1}$. A Hamamatsu R3809U Micro Channel plate (MCP) detector was used to record the fluorescence. For time-resolved measurements, both the MCP signal and pulses from a trigger photodiode monitoring the pump beam were passed through constant fraction discriminators. The time lag between the MCP signal and trigger was fed to a multi-channel analyzer as a voltage generated by a time to amplitude converter (TAC). The MCP-pulses (average rate of $\lesssim 10^4\ \mathrm{s}^{-1}$) were used as TAC start pulses, while the trigger-diode output was connected to the TAC stop input. This time-correlated single-photon counting technique provides a resolution of 55 ps.

In order to verify the quantum efficiency of dye on titania, we measured the luminescence decay of dye on a powder of anatase titania particles (Aldrich). For R6G on titania (see Fig. 3) we find a very fast decay, characterized by a ~ 500 ps decay time. After rapid decay over ~ 1 decade, a slower time tail sets in. The luminescence decay of R6G dissolved in ethanol, on the other hand, is observed to be single-exponential with a decay time of 3.6 ns, as expected from literature [39]. Evidently, the quantum efficiency of R6G on titania is strongly reduced compared to the $\sim 95\%$ quantum efficiency in ethanol. We use the first moment of the decay curve as a measure of the decay time. Comparison to the expected radiative decay rate $(3.6\ \mathrm{ns})^{-1}$ yields an estimate of the quantum efficiency less than 10% [40, 41]. The relevant nonradiative decay mechanism for organic dyes on semiconductors is a well-documented electron-transfer process [42]. In this process the excited state of the dye has an energy above the conduction band of the TiO_2 to which it is adsorbed. After excitation the excited electron is transferred to the semiconductor, leaving the dye molecule oxidized. This efficient electron transfer process is the basis of the so-called 'organic solar cell' developed by O' Regan and Grätzel [43]. The oxazine dye Nile Blue has a low quantum efficiency $\lesssim 15\%$ both in solution [29] and on titania. Several schemes were considered to prevent the electron transfer in order to retain a high quantum efficiency. Any scheme in which the dye is incorporated in the crystal (for instance incorporated in small SiO_2 spheres) before the titania is formed is incompatible with the heating stage necessary to form and crystallize the titania, as dyes generally do not withstand temperatures in excess of 350 °C. Coating of the TiO_2 surface with a ~ 5 nm layer of SiO_2 prior to adsorbing the dye was demonstrated to prevent the electron transfer in the case of titania powders [41]. New methods are currently being developed to coat the inner surface of the titania air sphere crystals with such an insulating layer [44]. Given the low quantum efficiency of dyes on titania, we have designed a cw experiment to probe the photonic DOS.

As alternative luminescent species, quantum dots or lanthanide ions may be considered. Unfortunately, typical quantum dots are not stable when exposed to air and water, do not usually have a

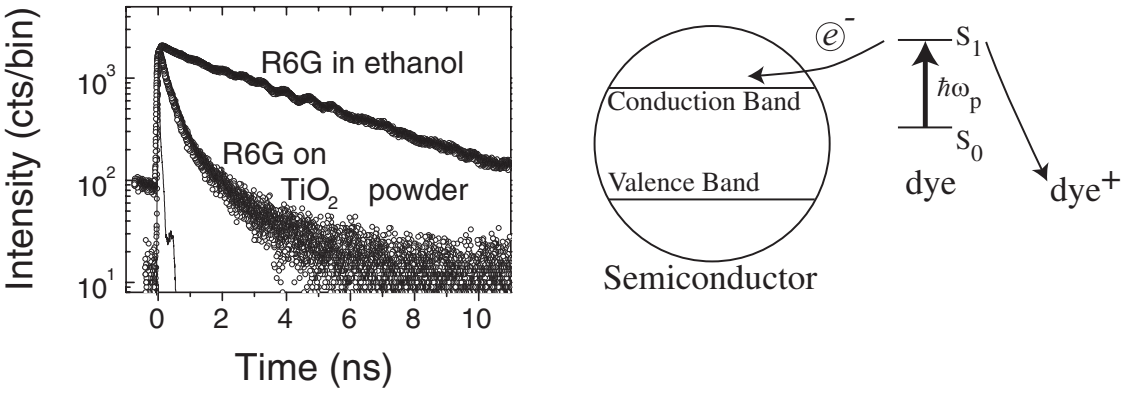

Fig. 3 a) The decay of R6G adsorbed on titania powder is very fast compared to the single-exponential decay of R6G dissolved in ethanol (3.6 ns lifetime). The instrument response is shown for comparison (thin line). b) Titania caused nonradiative decay of dye by electron transfer; the excited electron is transferred to the conduction band of the semiconductor, leaving the dye oxidized.

quantum efficiency near unity, and may not be immune to electron transfer processes [45]. Still, quantum dots with inorganic coating (such as CdSe–ZnS/ZnSe/ZnS/CdS core-shell nanocrystals) to passivate the surface electronically and chemically appear to be among the most promising and flexible light sources for future experiments [46–48]. Rare earth ions on the other hand have the disadvantage of not providing a inhomogeneously broadened spectrum. Their narrow spectrum compared to the large bandwidth of the L-gap and pseudo gap, would necessitate a much larger set of lattice spacings a to map the LDOS over the normalized frequency ($\omega a/2\pi c$) range of interest. Furthermore, the efficiency of luminescence for rare earth ions strongly depends on the chemical environment, and is not well studied for titania hosts. Typically efficient emission is obtained only after shielding the ions, using organic ligands for instance [49, 50]. Furthermore, the long radiative lifetimes (millisecond range) of rare earth ions will not facilitate cavity QED in the strong coupling limit, once a photonic band gap has been achieved.

5 Inhibition of emission and the DOS

Emission spectra at several detection angles for a R6G doped crystal with $a = 480$ nm are presented in Fig. 4. Internal Bragg diffraction of the diffusely propagating luminescence causes clearly observable stop bands suppressing the spectra in angle dependent frequency ranges, as apparent in Fig. 4a. Before discussing the connection between angle-dependent, angle-integrated and reference emission spectra, it is instructive to discuss the experimental signatures indicative of bad sample quality. Lineshapes reported on in this paper (apart from Fig. 4b) are from samples with $a = 430$, 480 and 510 nm which showed clear stop gaps and well reproducing line shapes over extended sample areas. Of the many crystals with these lattice parameters examined in the experiment, a fraction $\lesssim 30\%$ was found for which emission spectra did not show any signature of photonic behavior, and several samples showed both areas resulting in clear stop gaps, and apparently disordered areas. In the latter cases, no stop gaps or gaps with depths less than 10% were found to affect the spectra, as apparent in Fig. 4b ($a = 480$ nm, R6G doped sample). Visual inspection of such samples or sample areas showed only faint or no opalescence, and SEM and optical microscopy indicated that large unstructured lumps of titania covered the sample surfaces. Such lumps may have been formed where the polystyrene template did not stick to the capillary walls during infiltration with the TiO_2 precursor. Emission lineshapes from these crystals, for which the fabrication was apparently not satisfactory, significantly differ from the emission lineshapes observed at any angle for the obviously photonic samples. Although lack of stop gaps or opalescence, and the observation of solid titania chunks only provide

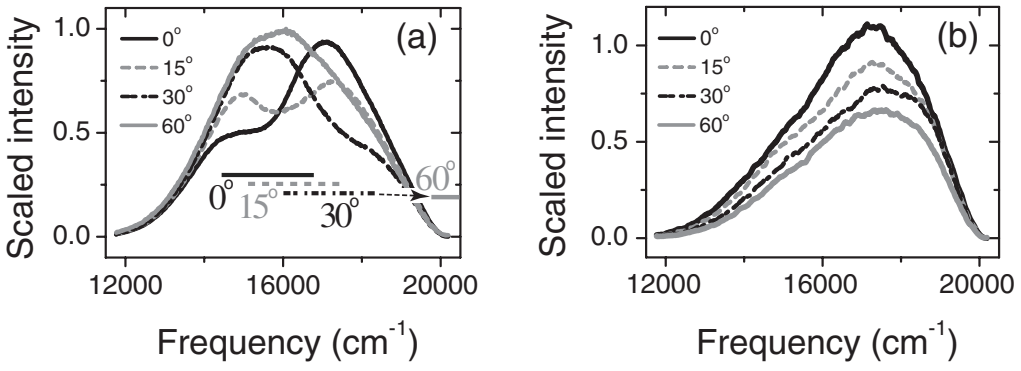

Fig. 4 a) Internal Bragg diffraction causes strongly angle dependent emission spectra from well ordered photonic crystals (R6G, $a = 480$ nm). Attenuation occurs in frequency bands indicated by horizontal bars, that shift to higher frequency according to the dispersion relation. b) Emission spectra of R6G on a apparently disordered sample made from a template with the same sphere size. No visible opalescence was discernible from the area coincident with the pump- and detection focus.

information on surface quality, we regard these crystals as apparently disordered. Emission spectra from the apparently disordered samples resemble spectra from dye in the reference hosts, apart from a broadening. We note that crystals with bad surface quality can not be surface-selectively bleached by using a pump beam at the Bragg angle. Sets of spectra without stop gaps may therefore be mixtures of emission from dye near the surface, from dye in disordered, and from dye in ordered air sphere arrays. The 'photonic' spectra presented in this paper were reproduced over sample areas at least ($\sim$0.5 mm)^2 in size, as probed by measuring lineshapes at many angles for a detection focus that was systematically scanned over grids with spacings 50 to 100 μm over the sample surfaces.

Figure 4a shows that the frequency range in which spectra are suppressed due to Bragg diffraction shifts to higher frequencies with increasing angle. Modification of the spectra ceased for angles α exceeding 60°. The line shapes were independent of pump intensity, and the emission intensity was found to increase in proportion to the pump power. The $\alpha \geq 60°$ spectra are representative of the angle-averaged total emission power, as discussed below. The $\alpha = 60°$ spectra for R6G doped samples with $a = 430$, 480 nm differ significantly from spectra of R6G in reference samples with $a = 350$ nm, as shown in Fig. 5a. A sizable reduction of emission power in the frequency window from $\sim$15500 to 20000 cm^{-1} is apparent when the spectra are scaled to match on the low frequency side below any Bragg condition. The reduction, which occurs in a frequency window blue shifted relative to the L-gap, results in clear red shifts of the maximum emission frequencies. A similar spectral shift was observed when comparing $\alpha = 60°$ spectra of the Nile Blue sample ($a = 510$ nm) with its reference, see Fig. 5b. The reference line shapes reproduced well on a multitude of reference samples, and were independent of angle, due to the fact that the lowest order Bragg diffraction occurs at 22000 cm^{-1}, far above the dye emission frequencies. The reduction is not due to differences in chemical interactions of the dye with its environment, since the reference samples are chemically identical to the photonic samples. Red shifts due to self absorption are excluded, since the dye concentrations were sufficiently low by at least two orders of magnitude.

We extract the photonic LDOS effect on the total emission by dividing the $\alpha = 60°$ spectra by the emission spectrum of the same dye in the reference samples, as shown in Fig. 6a for the R6G data sets with $a = 480$, 430 nm, and for the Nile Blue sample with $a = 510$ nm in Fig. 6b. Due to the low efficiency of these dyes on titania, the intensity ratios, which are scaled to unity on the low frequency shoulder, represent the LDOS probed by the dye, divided by the reference LDOS. The lowest order stop gap of the reference samples at 22000 cm^{-1} is far above the dye spectrum. Hence, the reference LDOS has a well defined quadratic frequency dependence [51, 22]. The width of the inhibition range

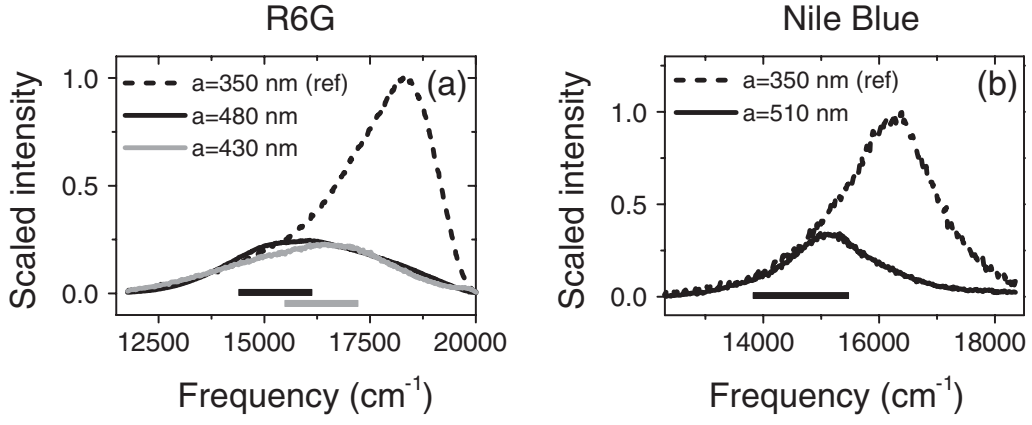

Fig. 5 a) Emission spectra of R6G in TiO_2 inverse opals with $a = 430$, 480 nm (grey, resp. black) detected at $\alpha = 60°$ strongly differ from the angle-independent emission spectrum of R6G in a TiO_2 inverse opals with $a = 350$ nm (not photonic in the frequency range shown). b) same for Nile Blue on a sample with $a = 510$ nm (black curve) and in the reference ($a = 350$ nm, dashed curve). Horizontal bars in both panels indicate the relevant L-gaps (stop bands at $\alpha = 0°$).

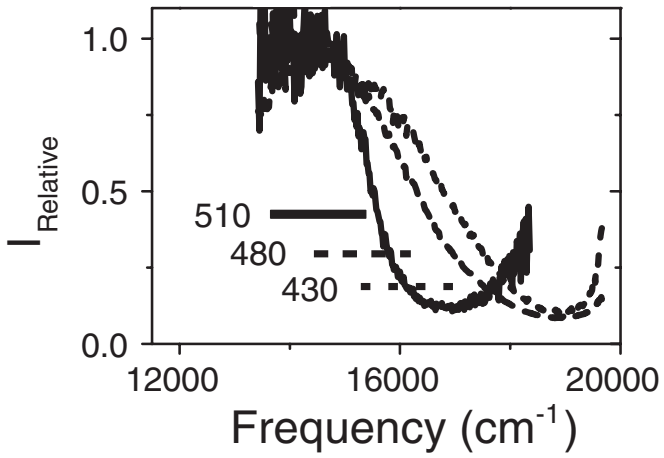

Fig. 6 Intensity ratios of spectra in Fig. 5 to the reference spectrum for R6G, with $a = 480$ nm (dashed) and $a = 430$ nm (dotted) and Nile Blue, for $a = 510$ nm to the Nile Blue reference spectrum. The inhibition shifts to the red with increasing lattice constant a. Horizontal bars indicate the L-gaps.

~ 2000 cm^{-1}, i.e., 13% of the L-gap center frequency, attests to the strongly photonic character of the inverse opals, which is robust to disorder in the range of the pseudo gap [52]. The inhibition range is blue shifted relative to the L-gap. This blue shift of the minimum in DOS relative to the L-gap is expected from plane wave calculations (see Fig. 8b and Ref. [22]), and may be simply understood from a consideration of the number of simultaneously excluded modes as a function of frequency. Indeed, from a simple angle-dependent stop-gap consideration one expects that the blue edge of the L-gap corresponds to the frequency for which the largest fraction of solid angle is simultaneously contained in a stop gap [33, 53]. The shift of the inhibition to higher frequency with smaller lattice parameter confirms that the spectral changes are due to the photonic crystal properties.

6 Effect of disorder on emission spectra

A crucial observation is that the $\alpha = 60°$ spectra are representative of the spectral distribution of angle-averaged luminescence in the bulk. The key mechanism determining the angle-dependent spectra is due to disorder effects. The optical effect of disorder is gauged by the transport mean-free path [54], which is the distance over which the direction of propagation of light is randomized due to scattering. For opals and inverse opals the transport mean-free path ℓ was recently determined from enhanced backscattering measurements [55]. Since the transport mean-free path $\ell \sim 15\,\mu$m is much smaller than the sample thickness $L \sim 200\,\mu$m, the luminescence propagates diffusively through the bulk of the crystals (see Fig. 7). The opposite case $\ell > L$ is relevant both for thin strongly photonic crystals and for all weakly photonic systems and has been analyzed by Megens et al. [37]. For $\ell > L$, single scattering of emission by defects at the external crystal interface is dominant, instead of multiple scattering in the bulk.

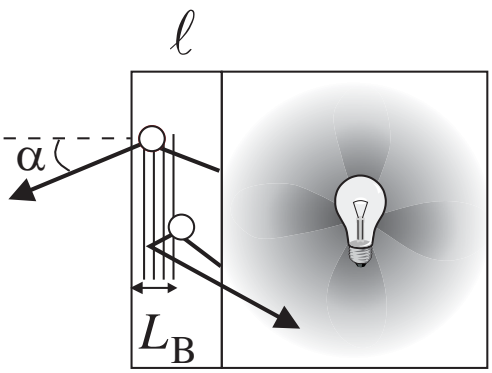

Fig. 7 (Schematic) Each individual source has a position dependent radiation pattern, determined by the Bloch modes available at the source position. Directional properties of each source are washed out by multiple scattering over length scales ℓ. Near the external interface the crystal planes internally diffract the diffuse luminescence, giving rise to stop bands in the spectra. The relevant length scale for internal diffraction is the Bragg attenuation length L_B, which is ~ 5 times smaller than the mean free path ℓ.

Even though different sources can have different radiation patterns, owing to their different local photonic environment, none of these directional properties of each source inside the photonic crystal reaches the observer. Instead, emission from all sources propagates diffusively to the crystal interface. The spectral distribution $I(\omega)$ of the diffuse luminescence in the bulk is the 4π sr average of spectra of all sources in the pump volume, and is thus determined only by the LDOS and the inhomogeneous line broadening of the dye. The diffuse luminescence acquires an angular dependence only when it exits the sample. This angle and frequency dependent modification of the diffuse luminescence spectrum is due to internal Bragg diffraction [38] and may be calculated from diffusion theory with internal reflection [56–58]. The relevant theory and experiments verifying the applicability of this theory using diffuse light injected by externally incident plane waves will be presented in Ref. [59]. According to diffusion theory, the diffuse intensity escaping in an angular range α to $\alpha + \mathrm{d}\alpha$ equals $\frac{3}{2} I(\omega) \cos\alpha [\tau_e(\omega) + \cos\alpha] [1 - R(\alpha, \omega)] \,\mathrm{d}(\cos\alpha)$. For exit angles *outside* a stop gap (i.e. $\alpha \geq 60^\circ$), the internal reflection coefficient $R(\alpha, \omega)$ vanishes for all emission frequencies. Hence, the frequency dependence of the measured spectrum at $\alpha \geq 60^\circ$ is only determined by the angle-integrated emission spectrum $I(\omega)$, and the so-called extrapolation length ratio $\tau_e(\omega)$. This frequency dependent parameter is related to an angle and polarization averaged internal reflection coefficient [57, 58], and can be derived from $R(\alpha, \omega)$ (see Ref. [57], Eq. (2.22) and (3.5–3.9)).

We estimate the internal reflection coefficient $R(\alpha, \omega)$ to be less than 70% for directions within a stop gap, and 0% outside. This estimate is based on the ratio of the mean free path ℓ to the Bragg attenuation length L_B, as first proposed in Ref. [38]. The mean free path ℓ is larger than the exponential attenuation length L_B associated with Bragg diffraction (typically $L_B/\ell \sim 0.2$–0.5). Intensity scattered at a distance $z < L_B$ less than the Bragg attenuation length from the interface is hardly Bragg diffracted. On the other hand the remaining fraction $(1 - L_B/\ell)$ for which the last scattering event occurs in the range $L_B < z < \ell$ propagates a sufficient distance to develop a stop band due to internal Bragg diffraction. This simple model predicts a total attenuation in the stop band equal to $R = 1 - L_B/\ell = 50\%$ to 80%, in agreement with the experiment. For $\alpha = 60^\circ$, we find that the extraction efficiency $(\tau_e(\omega) + \frac{1}{2})$ increases by less than 30% as the frequency increases from the red to the blue edge of the L-gap, and linearly decreases by less than 10% as the frequency is increased to the blue edge of the emission spectra. Consequently, the $\alpha = 60^\circ$ emission spectra are representative of the diffuse luminescence spectra $I(\omega)$ in the bulk to within better than 30%. Therefore the large difference up to a factor 5 between the $\alpha = 60^\circ$ emission spectra from the photonic crystals and reference spectra in Fig. 5 must be due to a large change in the angle-integrated total emission power, due to modulation of the photonic LDOS. Detailed analysis shows that the true inhibition of total emission may even exceed the lineshape ratio in Fig. 6, due to a slightly enhanced extraction efficiency for $\alpha = 60^\circ$ for frequencies in the inhibition band.

For comparison with the cw experiment, we have performed time resolved measurements for the Nile Blue doped samples, shown in Fig. 8a. No significant difference is apparent between total decay rates in the photonic crystal and the reference, neither for frequencies below or in the range of inhibited radiative decay evident from the spectra. It appears that the low quantum efficiency precludes determination of the radiative decay rate from a dynamic measurement, but allows to extract changes in radiative decay rate from the emitted power. A lengthening of the radiative lifetime according to the inhibition in Fig. 6, causes a variation $\lesssim 10\%$ of the total lifetime for a quantum efficiency of 10%. Lacking efficient emitters on semiconductors such as TiO_2 [42], the complementary experiments in which a lengthening of the total lifetime is expected currently remain out of reach. In view of the large magnitude of the inhibition of emission on titania, recently developed silica, zirconia and alumina air sphere crystals may prove to be sufficiently photonic for such experiments, despite the lower index contrast [60]. These host materials do not cause quenching by electron transfer.

Remarkably, the magnitude of the reduction in emitted power, amounting to at least a factor 5 relative to the low frequency edge, exceeds the reduction in total solid angle for light propagation by a factor 2, which is a simple estimate of the reduction of the total DOS [33]. To investigate this further we have calculated the total DOS using the H-field inverted matrix technique [22, 61], and a special-point fcc Brillouin zone integration scheme [62]. Eigenfrequencies were calculated using

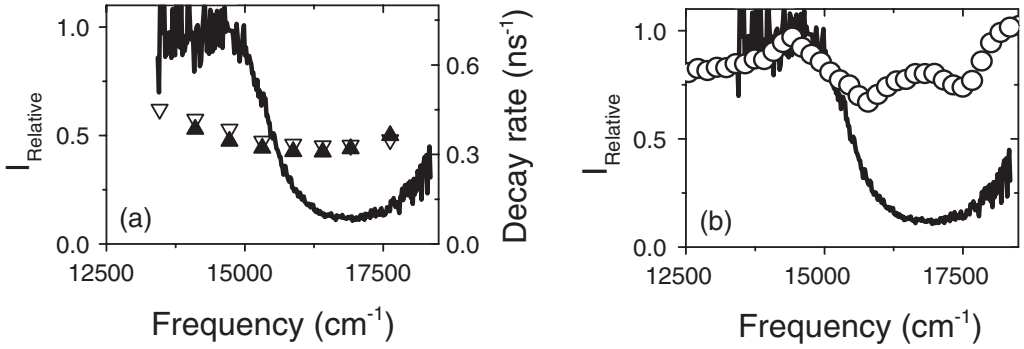

Fig. 8 a) Intensity ratio for $a = 510$ nm (Nile Blue, black curve) taken from Fig. 6. For comparison the spectrally resolved fluorescence decay rates are shown of Nile Blue in the reference (closed triangles) and photonic crystal (open triangles). No significant difference is observed, due to the low quantum efficiency. b) Black curve as in (a). The open circles indicate the total DOS calculated for a titania inverse opal $a = 510$ nm, divided by ω^2 and scaled to match on the low frequency edge.

725 plane waves, and a coarse grid of 2480 k-points spanning the irreducible part of the Brillouin zone. As a model for the distribution of dielectric material, we assume close packed air spheres surrounded by shells of titania ($\epsilon = 6.5$) with cylindrical windows connecting neighboring spheres. In units of the close packed sphere radius r, we assume shells of inner radius r, outer radius $1.09r$ and window radius $0.4r$. This model corresponds to a volume fraction of 10.7% of solid material and the structure is consistent with scanning electron microscope observations. The corresponding band structure predicts reflectivity features in excellent agreement with prior experiments [34, 63], both in the range of first and second order Bragg diffraction (i.e. up to band 9). As shown in Fig. 8(b), the total DOS normalized by the quadratic DOS in the reference samples is reduced in a frequency range coincident with the experimentally determined inhibition window. The modulation of the total DOS, however, amounts to even less than the factor of two estimated from the reduction in total solid angle of allowed propagation directions. Clearly, a complete understanding of the large reduction of the emitted power requires a full calculation of the *local* DOS, taking the spatial distribution and dipole orientation of the emitters into account. In our experiment, the spatial distribution of emitters limits the probe volume to those $\sim 10\%$ of the unit cell occupied by titania. Future experiments using, e.g., atomic vapors as emitters, will allow us to probe the local DOS over the remaining unit cell volume. Calculating the local DOS averaged over *part of* the unit cell currently remains a formidable task beyond the scope of this paper. As yet, the local DOS of realistic three-dimensional structures has only been theoretically studied for a limited number of dipole positions by a few groups [22, 51, 64]. We note that a time-resolved decay measurement for efficient fluorescent sources would not show a simple single exponential decay, but be composed of contributions from sources with different decay times depending on the LDOS at their positions. The first moment of the intensity distribution over time should correspond to the source-averaged reduction in emission power reported in this paper. In view of the expected complexity of the fluorescence decay of ensembles of sources, it is of prime importance to develop combinations of light sources and photonic crystal materials for which the decay dynamics in absence of LDOS variations is completely understood, and which feature a high quantum efficiency.

7 Conclusion

We have presented a detailed discussion of our recent experiment [17] that for the first time demonstrates broadband inhibition of spontaneous emission in a large spatial volume limited only by the size of our photonic crystals. This is a major step towards realizing novel quantum electrodynamics in controlled 3D defect cavities that are shielded from vacuum fluctuations. It is expected that pro-

nounced maxima in the DOS of photonic crystals will be useful in applications requiring enhanced spontaneous emission in large spatial volumes [1, 8]. In fact the observed large inhibition compared to the expected variation of the total DOS shows that far reaching spontaneous emission control may even be realized without a full photonic band gap. Central issues to master such control, however, revolve around quantitative knowledge of the local density of states throughout the unit cell, control over the locations of the emitters, and most importantly the luminescence quantum efficiency. Each photonic crystal backbone material, usually chosen on the merit of large real and small imaginary dielectric constant, will pose different challenges if efficient emitters are called for. The electron transfer processes occurring on semiconductors like titania simply present an illustrative example of such a specific constraint due to materials issues. Finally, we have shown the extraordinary relevance of structural disorder in the interpretation of emission experiments.

Acknowledgements We thank Henry Schriemer for contributions early in the project. This work is part of the research program of the ''Stichting voor Fundamenteel Onderzoek der Materie (FOM),'' which is financially supported by the ''Nederlandse Organisatie voor Wetenschappelijk Onderzoek (NWO).''

References

[1] S. Haroche, in: Systèmes Fondamentaux en Optique Quantique/Fundamental Systems in Quantum Optics, edited by J. Dalibard, J. M. Raimond, and J. Zinn-Justin (North-Holland, Amsterdam, 1992), pp. 767.
[2] K. H. Drexhage, H. Kuhn, and F. P. Schäfer, Ber. Bunsenges. Phys. Chem. **72**, 329 (1968).
[3] D. J. Heinzen, J. J. Childs, J. E. Thomas, and M. S. Feld, Phys. Rev. Lett. **58**, 1320 (1987).
[4] A. J. Campillo, J. D. Eversole, and H.-B. Lin, Phys. Rev. Lett. **67**, 437 (1991).
[5] P. Andrew and W. L. Barnes, Science **290**, 785 (2000).
[6] E. Yablonovitch, Phys. Rev. Lett. **58**, 2059 (1987).
[7] C. M. Soukoulis (ed.), Photonic Band Gap Materials (Kluwer Academic Publishers, Dordrecht, 1996).
[8] C. M. Soukoulis (ed.), Photonic Crystals and Light Localization in the 21st Century (Kluwer Academic Publishers, Dordrecht, 2001).
[9] J. Martorell and N. M. Lawandy, Phys. Rev. Lett. **65**, 1877 (1990).
[10] E. P. Petrov, V. N. Bogomolov, I. I. Kalosha, and S. V. Gaponenko, Acta Phys. Pol. A **94**, 761 (1998).
[11] M. Megens, J. E. G. J. Wijnhoven, A. Lagendijk, and W. L. Vos, Phys. Rev. A **59**, 4727 (1999).
[12] Z. Y. Li and Z. Q. Zhang, Phys. Rev. B **63**, 125106 (2001).
[13] S. V. Gaponenko, A. M. Kapitonov, V. N. Bogomolov, A. V. Prokofiev, A. Eychmuller, and A. L. Rogach, JETP Lett. **68**, 142 (1998).
[14] K. Yoshino, S. B. Lee, S. Tatsuhara, Y. Kawagishi, M. Ozaki, and A. A. Zakhidov, Appl. Phys. Lett. **73**, 3506 (1998).
[15] A. Blanco, C. López, R. Mayoral, H. Míguez, F. Meseguer, A. Mifsud, and J. Herrero, Appl. Phys. Lett. **73**, 1781 (1998).
[16] S. G. Romanov, T. Maka, C. M. Sotomayor-Torres, M. Müller, and R. Zentel, J. Appl. Phys. **91**, 9426 (2002).
[17] A. F. Koenderink, L. Bechger, H. P. Schriemer, A. Lagendijk, and W. L. Vos, Phys. Rev. Lett. **88**, 143903 (2002).
[18] R. Sprik, B. A. van Tiggelen, and A. Lagendijk, Europhys. Lett. **35**, 265 (1996).
[19] J. E. G. J. Wijnhoven and W. L. Vos, Science **281**, 802 (1998).
[20] E. Fermi, Rev. Mod. Phys. **4**, 87 (1932).
R. Loudon, The Quantum Theory of Light, 2nd ed. (Oxford University Press, England, 1983).
[21] N. Vats, S. John, and K. Busch, Phys. Rev. A **65**, 043808 (2002).
[22] K. Busch and S. John, Phys. Rev. E **58**, 3896 (1998).
[23] D. V. van Coevorden, Light Propagation in Ordered and Disordered Media, Ph.D. thesis, (University of Amsterdam 1997).
[24] J. D. Jackson, Classical Electrodynamics (John Wiley and Sons, New York, 1975).
[25] Y. Xu, R. K. Lee, and A. Yariv, Phys. Rev. A **61**, 033807 (2000).
[26] B. Y. Tong, P. K. John, Y. T. Zhu, Y. S. Liu, S. K. Wond, and W. R. Ware, J. Opt. Soc. Amer. B **10**, 356 (1993).
[27] R. H. J. Kop, P. de Vries, R. Sprik, and A. Lagendijk, Phys. Rev. Lett. **79**, 4369 (1997).

[28] B. A. van Tiggelen and E. Kogan, Phys. Rev. A **49**, 708 (1994).
[29] U. Brackmann, Lambdachrome Laser Dyes (Lambda Physik GmbH, Göttingen, 1997).
[30] J. E. G. J. Wijnhoven, L. Bechger, and W. L. Vos, Chem. Mater. **13**, 4486 (2001).
[31] E. D. Palik (ed), Handbook of Optical Constants of Solids (Academic Press, New York, 1952).
[32] J. F. Galisteo López and W. L. Vos, Phys. Rev. E **66**, 036616 (2002).
[33] M. S. Thijssen, R. Sprik, J. E. G. J. Wijnhoven, M. Megens, T. Narayanan, A. Lagendijk, and W. L. Vos, Phys. Rev. Lett. **83**, 2730 (1999).
[34] H. M. van Driel and W. L. Vos, Phys. Rev. B **62**, 9872 (2000).
[35] P. C. Becker, H. L. Fragnito, J. Y. Bigot, C. H. Brito Cruz, R. L. Fork, and C. V. Shank, Phys. Rev. Lett. **63**, 505 (1989).
[36] M. D. Barnes, W. B. Whitten, S. Arnold, and J. M. Ramsey, J. Chem. Phys. **97**, 7842 (1992).
[37] M. Megens, J. E. G. J. Wijnhoven, A. Lagendijk, and W. L. Vos, J. Opt. Soc. Am. B **16**, 1403 (1999).
[38] H. P. Schriemer, H. M. van Driel, A. F. Koenderink, and W. L. Vos, Phys. Rev. A **63**, 011801 (2001).
[39] P. R. Hammond, J. Chem. Phys. **70**, 3884 (1979).
[40] R. G. Kubin and A. N. Fletcher, J. Lumin. **27**, 455 (1982).
[41] L. Bechger, A. F. Koenderink, and W. L. Vos, Langmuir **18**, 2444 (2002).
[42] P. V. Kamat, Chem. Rev. **93**, 267 (1993).
[43] B. O' Regan and M. Grätzel, Nature **353**, 737 (1991).
[44] L. Bechger and W. L. Vos, submitted (2002).
[45] E. P. A. M. Bakkers, E. Reitsma, J. J. Kelly, and D. Vanmaekelbergh, J. Phys. Chem. B **103**, 2781 (1999).
[46] C. B. Murray, D. J. Norris, and M. G. Bawendi, J. Am. Chem. Soc. **115**, 8706 (1993).
[47] B. O. Dabbousi, J. Rodriguez-Viejo, F. V. Mikulec, J. R. Heine, H. Mattousi, R. Ober, K. F. Jensen, and M. G. Bawendi, J. Phys. Chem. B **101**, 9463 (1997).
[48] X. Peng, M. C. Schlamp, V. Kadavanich, and A. P. Alivisatos, J. Am. Chem. Soc **119**, 7019 (1997).
[49] F. J. P. Schuurmans, Light in Complex Dielectrics, Ph.D. thesis, University of Amsterdam (1999).
[50] A. Polman, Physica B **300**, 78 (2001).
[51] T. Suzuki and P. K. L. Yu, J. Opt. Soc. Amer. B **12**, 570 (1995).
[52] Z. Y. Li and Z. Q. Zhang, Phys. Rev. B **62**, 1516 (2000).
[53] M. Megens, H. P. Schriemer, A. Lagendijk, and W. L. Vos, Phys. Rev. Lett. **83**, 5401 (1999).
[54] A. Ishimaru, Wave Propagation and Scattering in Random Media (Academic Press, New York, 1978).
[55] A. F. Koenderink, M. Megens, G. van Soest, W. L. Vos, and A. Lagendijk, Phys. Lett. A **268**, 104 (2000).
[56] A. Lagendijk, R. Vreeker, and P. de Vries, Phys. Lett. A **136**, 81 (1989).
[57] J. X. Zhu, D. J. Pine, and D. A. Weitz, Phys. Rev. A **44**, 3948 (1991).
[58] D. J. Durian, Phys. Rev. E **50**, 857 (1994).
[59] A. F. Koenderink and W. L. Vos, Phys. Rev. Lett., submitted (2002).
[60] L. Bechger, P. Lodahl, A. F. Koenderink, and W. L. Vos, in preparation (2003).
[61] H. S. Sözüer, J. W. Haus, and R. Inguva, Phys. Rev. B **45**, 13962 (1992).
[62] H. J. Monkhorst and J. D. Pack, Phys. Rev. B **13**, 5188 (1976).
[63] W. L. Vos and H. M. van Driel, Phys. Lett. A **272**, 101 (2000).
[64] Z. Y. Li, L. L. Lin, and Z. Q. Zhang, Phys. Rev. Lett. **84**, 4341 (2000).